Nanoscale Advances

PAPER

View Article Online
View Journal | View Issue

Cite this: *Nanoscale Adv.*, 2021, **3**, 805

Nitrogen-doped carbon dots for sensitive detection of ferric ions and monohydrogen phosphate by the naked eye and imaging in living cells†

Qiaoling Liu,* Borong Ren, Kaixin Xie, Yanmei Yan, Ruirong Liu, Shiyou Lv, Qing He, Boru Yang and Lin Li*

Received 13th September 2020
Accepted 3rd December 2020

DOI: 10.1039/d0na00769b

rsc.li/nanoscale-advances

Nitrogen doped carbon dots (N-CDs) have been prepared *via* a one-pot hydrothermal method by using formamide and *o*-phenylenediamine as the carbon precursors. The as-fabricated N-CDs display excellent water dispersibility, good biocompatibility and anti-photobleaching properties. A strong emission band with an emission maximum ($\lambda^{\mathrm{fl}}_{\mathrm{max}}$) of 556 nm is observed under 450 nm excitation, and a large Stokes shift of 106 nm is presented. However, the fluorescence is quenched by the addition of Fe^{3+}; a good linearity is shown in the range of 0–65 μM with a detection limit as low as 0.85 μM. Fortunately, the quenched fluorescence could be recovered rapidly by the addition of monohydrogen phosphate (HPO_4^{2-}) due to the formation of the stable [N-CDs–Fe^{3+}–HPO_4^{2-}] complex, and a good linearity is exhibited in the range of 0–60 μM with a low detection limit of 0.80 μM for HPO_4^{2-}. A novel "on–off–on" fluorescence response is seen with an obvious color change from yellow-crimson-yellow by the naked eye. In addition, the confocal microscopy images suggest that the as-synthesized N-CDs could serve as a sensitive nanosensor for Fe^{3+} and HPO_4^{2-} detection, implying the diverse potential application of N-CDs in the biomedical field.

Introduction

Fe^{3+} ions as essential transition metal ions for basic life activities play vital roles in many physiological and pathological processes, such as oxygen transport, enzyme catalysis,[1] cellular metabolism,[2] and gene expression.[3,4] The deficiency of iron will cause iron deficiency anemia and related diseases.[5] However, excess of body iron has potential hazards of generation of free radicals that would result in cell damage and oxidative stress,[6] and further lead to metabolism disorder and cancer,[7] liver and kidney damage,[8] and Huntington's, Parkinson's and Alzheimer's diseases.[9,10] Therefore, it is urgent to develop an efficient method to monitor the change of Fe^{3+} concentration *in vivo* for better understanding its regulation mechanism and physiological process.

On the other hand, phosphorus as a control element participates in many vital processes, such as signal transduction and energy storage.[11,12] In body fluids, phosphorus is in the form of dihydrogen phosphate/monohydrogen phosphate ($H_2PO_4^{-}/HPO_4^{2-}$) with a ratio of 1 : 4,[13] and they could be transformed into each other at different physiological pH from 5.0 to 9.0. Deficiency of phosphate may induce many serious problems, such as growth retardation, rickets and osteomalacia,[14] metabolism disorder, and Parkinson's and Alzheimer's disease.[15,16] Herein, an important problem is that both Fe^{3+} and phosphate could lead to the same diseases, including metabolism disorder, and Parkinson's and Alzheimer's disease. Thus the design strategy is to explore a sensitive sensor to monitor both Fe^{3+} and HPO_4^{2-} in living systems for further understanding their interaction and relevant pathogenesis. However, it is a great challenge for us due to the high stability of Fe^{3+} and specific tetrahedral structure of phosphate ions.

Nowadays many methods based on fluorescence assay are designed for Fe^{3+} sensing. Compared to organic dyes and heavy metal based quantum dots, carbon dots exhibit many distinct advantages, such as excellent biocompatibility, high photostability, good water dispersion and environmental friendliness.[17,18] These special superiorities make them worthy candidates for their potential application in biomedical fields. Recently some carbon-dot based Fe^{3+} sensors have been reported.[19–30] Unfortunately, due to the intrinsic drawbacks of carbon dots, these carbon dots need UV excitation and their Stokes shifts are small,[28–30] which seriously restrict their application in living systems. As for HPO_4^{2-}, there is little information based on carbon dots for phosphate anion ($H_2PO_4^{-}/HPO_4^{2-}$) detection so far.

Herein, novel carbon dots have been developed *via* a one-pot hydrothermal method by using formamide and *o*-phenylenediamine as carbon precursors. The nitrogen-doped carbon

---

Department of Chemistry, Taiyuan Normal University, 319 University Street, Yuci District, Jinzhong 030619, P. R. China. E-mail: liuqiaoling@tynu.edu.cn; lilin@tynu.edu.cn; Tel: +86-351-2886580

† Electronic supplementary information (ESI) available: Optical properties of the N-CDs and the optimum reaction conditions. See DOI: 10.1039/d0na00769b

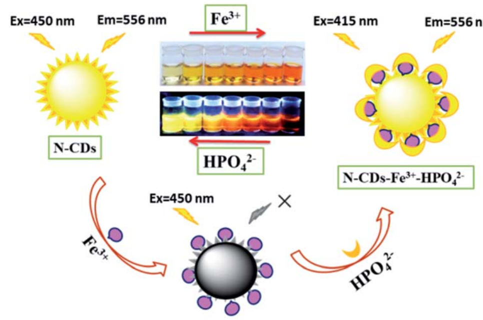

Scheme 1 Schematic illustration of the N-CDs as a nanosensor for the detection of Fe^{3+} and HPO_4^{2-} with obvious "on–off–on" fluorescence behaviour in aqueous solution.

dots (N-CDs) exhibit a large Stokes shift (more than 100 nm) under 450 nm excitation. With the addition of Fe^{3+}, a very obvious color change is observed from light yellow to crimson under daylight by the naked eye with distinct fluorescence quenching. While the fluorescence can be rapidly recovered after HPO_4^{2-} is added into the complex of N-CDs–Fe^{3+}, a sensitive "on–off–on" fluorescence response is presented with the color restoration (Scheme 1). Moreover, the confocal microscopy images suggest that the as-prepared carbon dots have the ability to monitor the changes of Fe^{3+} and HPO_4^{2-} concentrations in living cells.

Experimental

Materials

Formamide and *o*-phenylenediamine were purchased from Shanghai Aladdin Reagent Co., Ltd. The solutions of metal ions were prepared from their chloride salts of analytical grade apart from 0.10 M Hg^{2+} and Pb^{2+} solutions were prepared from their nitrates. Moreover, Fe^{2+} solution (0.10 M) was prepared just before use. Ultrapure water was acquired from a Heal Force SMART-N ultrapure water system (Heal Force, China). Human laryngeal epidermoid carcinoma (HEp-2) cells were obtained from Shanxi Medical University. Dulbecco's modified eagle medium (DMEM) and fetal bovine serum (FBS) were purchased from Gibco.

Apparatus

UV-vis absorption spectra were obtained on a UH4150 spectrophotometer (Hitachi, Japan). All fluorescence measurements were recorded on an F7000 spectrofluorometer (Hitachi, Japan) at room temperature. The FT-IR spectrum was obtained on a Nicolet NEXUS 670 spectrophotometer (USA). The X-ray photoelectron spectra (XPS) were obtained on a Thermo ESCALAB 250XI (Thermo Fisher Scientific, USA). Transmission electron microscopy (TEM) images were taken by using a Tecnai G2 F20 S-Twin (FEI, USA) with an accelerating voltage of 200 kV.

Cell cytotoxicity assay

The MTT assay was employed to assess the cytotoxicity of the N-CDs. Briefly, HEp-2 cells were seeded in 96-well plates (5×10^4 cells per well) and cultured in DMEM supplemented with 10% FBS and 100 U mL^{-1} penicillin–streptomycin at 37 °C in a 5% CO_2 humidified environment overnight. Then some of the cells were designated as a control group, and the others were treated with different concentrations of the N-CDs (0.25, 0.5, 0.75, 1.0 mg mL^{-1}). After 24 h of the N-CD exposure, the cells were carefully rinsed with 2-[4-(2-hydroxyethyl)piperazin-1-yl]ethanesulfonic acid (HEPES) buffer solution (25 mM, pH 7.2) three times, fresh growth medium (200 μL) containing MTT (5.0 mg mL^{-1}) was added into each well and then the cells were incubated for 4 h in a 5% CO_2 atmosphere at 37 °C. The growth medium was replaced by dimethyl sulfoxide (100 μL), and the absorption intensity of each well was measured at 490 nm.

Cell culture and imaging

HEp-2 cells were seeded in 35 mm glass bottom dishes and cultured in DMEM overnight before use. The next day, the cells were cultured with 1 mL of fresh medium containing 0.5 mg mL^{-1} N-CDs for 1 h at 37 °C in a 5% CO_2 humidified environment. Then the cells were washed with HEPES buffer solution (25 mM, pH 7.2) three times, and all of these cells were subjected to cell imaging with a ZEISS LSM 880 confocal laser scanning microscope (Germany) under 458 nm excitation. The emission signals were collected from 500 to 580 nm. After this, some of them were designated as the control group, and the others were treated with 140 μM of $FeCl_3$ solution in culture medium for 2 h, and these cells were subjected to cell imaging. After this the HEp-2 cells were further cultured with 140 μM of Na_2HPO_4 solution for 1 h at 37 °C and were imaged again.

Results and discussion

Synthesis of the N-CDs

The as-fabricated N-CDs were obtained by a one-pot hydrothermal method with formamide and *o*-phenylenediamine as carbon precursors, and the optimized reaction conditions are depicted in Fig. S1 and S2.† Briefly, *o*-phenylenediamine (0.1 g) and formamide (55 μL) were stirred and dissolved in 10 mL ethanol according to the molar ratio 1 : 1.5, and this solution was transferred into a 25 mL Teflon-lined autoclave and kept at 150 °C for 4 h. After this a deep yellow solution was obtained by cooling down naturally. Afterwards this crude product was purified by chromatography on a silica gel column with ethyl acetate/ethanol (40 : 1) as the eluent; the purified N-CDs were finally obtained with a 22 wt% yield.

Characterization of the N-CDs

The morphology, structure and composition of N-CDs are characterized by using high resolution transmission electron microscopy (HRTEM) and X-ray diffraction (XRD). As shown in Fig. 1, the average size of the N-CDs is 3.32 nm with a monodispersed spherical morphology. The HRTEM image exhibits good crystalline structures with a lattice spacing of 0.32 nm, which can be ascribed to the (002) lattice spacing of carbon-based materials. This deduction is further confirmed

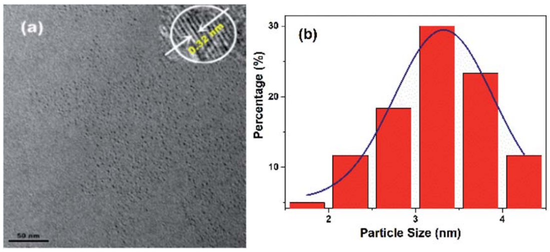

Fig. 1 (a) TEM image of the N-CDs (inset: corresponding HRTEM image). (b) The size distribution of the N-CDs.

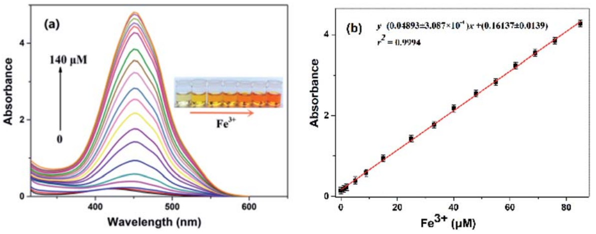

Fig. 2 (a) Absorption spectra of the N-CDs in pure water (0.04 mg mL^{-1}) with increased concentrations of Fe^{3+} (0–140 μM). The inset shows the image of the N-CDs in pure water with the increased Fe^{3+} from left to right under daylight. (b) Linear relationship between absorbance and the concentration of Fe^{3+}.

by X-ray diffraction analysis with a diffraction peak at *ca.* 26.5° (Fig. S3, ESI†).[31]

Subsequently, the surface functional groups and the elemental composition of the N-CDs are determined by X-ray photoelectron spectroscopy (XPS) and Fourier transform infrared (FT-IR) spectroscopy. The XPS spectrum of the N-CDs (Fig. S4a, ESI†) displays three major peaks at 285.3, 399.7, and 532.4 eV, which can be assigned to C 1s, N 1s and O 1s, respectively. The ratio of C, N and O is C 1s 76.21%, N 1s 13.12% and O 1s 10.68%. The high-resolution XPS spectrum of C 1s exhibits three peaks at 284.4, 285.0 and 285.6 eV, corresponding to C–C/C=C, C–N and O=C–O groups, respectively (Fig. S4b, ESI†).[29] The O 1s spectrum is fitted with three peaks at 531.6, 532.5 and 533.6 eV, suggesting the C=O, C–O and C–OH groups (Fig. S4c, ESI†).[32] The N 1s spectrum has three peaks at 398.5, 399.3 and 400.2 eV that are ascribed to C–N, C=N and N–H groups, respectively (Fig. S4d, ESI†).[19]

The XPS analyses of the N-CDs are in good agreement with FT-IR assignments (Fig. S5a, ESI†). The FTIR spectrum of the N-CDs displays sharp peaks at 3388 cm^{-1} and 1584 cm^{-1}, corresponding the stretching vibration and bending vibration of the N–H group, respectively.[33] The broad peak at 3185 cm^{-1} is ascribed to the stretching vibration band of the carboxyl group. The peaks at 2917 cm^{-1} and 2848 cm^{-1} are assigned to the C–H stretching vibrations of the amorphous carbon structure.[30] The peak at 1631 cm^{-1} is ascribed to the amide bonding from C=O stretching.[25] The sharp peak located at 1502 cm^{-1} is assigned to C=C from aromatic ring stretching vibration. Moreover, the peaks at 1458 cm^{-1}, 1269 cm^{-1}, 1152 cm^{-1} and 747 cm^{-1} originate from C=N, O–H, C–O/C–N and C–H stretching vibrations.[34,35] Both the XPS and FT-IR spectra suggest that the as-prepared N-CDs have a large number of amino groups and carboxyl groups on their surface.

Optical properties of the N-CDs for Fe^{3+} sensing

The optical properties of the N-CDs are examined using UV-vis and fluorescence emission spectra in pure water. The N-CDs show a weak absorption peak at 420 nm (Fig. 2a). With the addition of Fe^{3+} (0.0–140 μM), the absorbance of the N-CDs increases greatly by 24-fold, and the absorption peak (λ_{max}) presents a red shift and finally reaches 450 nm with quite an obvious color change from light yellow to crimson to the naked eye, indicating the formation of the N-CDs–Fe^{3+} complex. There is a good linearity between absorbance at 450 nm and the concentration of Fe^{3+} in the range of 0–85 μM (Fig. 2b), which means that the N-CDs have potential application for Fe^{3+} sensing.

The fluorescence characteristics of the N-CDs are explored in detail. An excitation-independent emission characteristic is exhibited with the increasing excitation wavelength from 390 nm to 490 nm (Fig. S6, ESI†), suggesting the stable and uniform distribution on the surface state of the N-CDs. Under 450 nm excitation, a strong fluorescence emission peak with an emission maximum (λ_{max}^{fl}) of 556 nm is presented, corresponding to free N-CDs (Fig. 3a), and the fluorescence quantum yield (φ) is 20% by using rhodamine B as a reference (eqn (1) of ESI†).[36] However, the fluorescence is gradually quenched with the increasing concentration of Fe^{3+} (0–140 μM); meanwhile the color of fluorescence changes from bright yellow to dark red under 365 nm UV lamp irradiation. The quenching efficiency $[(F_0 - F)/F_0]$ reveals a good linear relationship ($R^2 = 0.9993$) with the concentration of Fe^{3+} in a range of 0–65 μM, where F_0 and F are the fluorescence intensities of the N-CDs at 556 nm in the absence and presence of Fe^{3+}, respectively (Fig. 3b). The limit of detection is 0.85 μM based on the S/N = 3 method, which is much lower than the maximum concentration of Fe^{3+} in drinking water (~5.357 μM) permitted by the US Environmental Protection Agency (EPA),[37] suggesting that the as-synthesized N-CDs could serve as a sensitive nanosensor for Fe^{3+} detection.

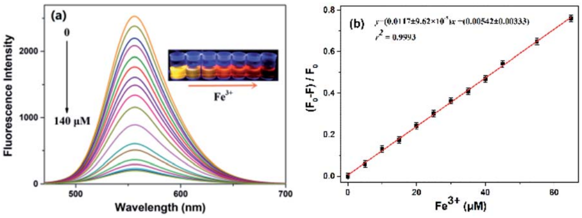

Fig. 3 (a) Fluorescence emission spectra of the N-CDs in pure water (0.04 mg mL^{-1}) with the different concentrations of Fe^{3+} (0–140 μM) under 450 nm excitation. The inset shows the image of the N-CDs in pure water with the increased Fe^{3+} from left to right under UV lamp irradiation at 365 nm. (b) Linear relationship between $[(F_0 - F)/F_0]$ and the concentrations of Fe^{3+}, where F_0 and F are the fluorescence intensities of the N-CDs at 556 nm in the absence and presence of Fe^{3+}, respectively.

Possible quenching mechanism

The quenching mechanism is discussed using Stern–Volmer eqn (1). The Stern–Volmer quenching constant (K_{sv}) is calculated using eqn (1) to be $2.95 \times 10^4\ M^{-1}$ at 298 K, which is very large and the quenching process by Fe^{3+} may be ascribed to the static quenching. In order to get insight into the quenching mechanism, the quenching constants at different temperatures (313 K and 323 K) are obtained (Fig. S7, ESI†). The K_{sv} exhibits a decreasing trend from $2.95 \times 10^4\ M^{-1}$ to $9.12 \times 10^3\ M^{-1}$ with the increasing temperature from 298 K to 323 K; thus the quenching process induced by Fe^{3+} may be due to the static quenching by the formation of the N/S-CDs–Fe^{3+} non-fluorescent complex.

$$F_0/F = 1 + K_{sv}[Q] \tag{1}$$

where K_{sv} and [Q] are the Stern–Volmer quenching constant and the concentration of Fe^{3+}, and F_0 and F are the fluorescence intensities of the N-CDs at 556 nm in the absence and presence of Fe^{3+}, respectively.

Furthermore, this speculation agrees with the result of the fluorescence lifetime (Fig. S8, ESI†). The average fluorescence lifetime of N-CDs is almost the same as the lifetime of the N-CDs–Fe^{3+} complex from 4.79 ns to 4.75 ns; thus the fluorescence quenching induced by Fe^{3+} might be attributed to the static quenching.

Optical properties of the N-CDs–Fe^{3+} for detection of HPO_4^{2-}

Fortunately, the quenched fluorescence can be recovered quickly in the presence of HPO_4^{2-}. Furthermore, the fluorescence intensity is even much higher by 1.3-fold increase than that of the free N-CDs when the concentration of HPO_4^{2-} is up to 140 μM (Fig. 4a), and the color of fluorescence also changes accordingly from dark red to bright yellow in the meantime (inset). The recovery efficiency $[(F_0 - F)/F_0]$ shows a good linear relationship ($R^2 = 0.9992$) with the concentration of HPO_4^{2-} in the range of 0–60 μM, where F_0 and F are the fluorescence intensities of the N-CDs–Fe^{3+} complex in the absence and presence of HPO_4^{2-}, respectively (Fig. 4b). The limit of detection for HPO_4^{2-} is determined to be as low as 0.80 μM, suggesting that the as-fabricated N-CDs are very sensitive for HPO_4^{2-}. Moreover, the highly reversible fluorescence responses of the N-CDs–Fe^{3+} to HPO_4^{2-} are observed, implying that the N-CDs are reusable for Fe^{3+} and HPO_4^{2-} detections (Fig. S9, ESI†). However, only HPO_4^{2-} couldn't cause any change in the fluorescence intensity and peak characteristics of the N-CDs.

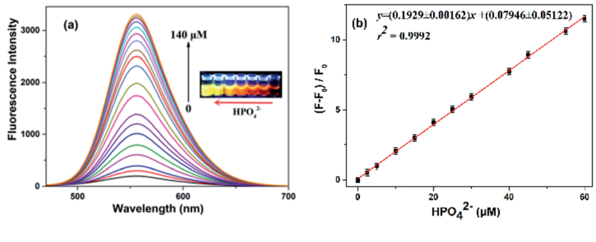

Fig. 4 (a) Fluorescence emission spectra of the N-CDs–Fe^{3+} complex in the presence of different concentrations of HPO_4^{2-} from 0 to 140 μM at an excitation wavelength of 450 nm. The inset is the image of the N-CDs–Fe^{3+} complex in pure water with the increased HPO_4^{2-} from right to left under UV lamp irradiation at 365 nm. (b) Linear relationship between $[(F - F_0)/F_0]$ and the concentration of HPO_4^{2-}, where F_0 and F are the fluorescence intensities of the N-CDs–Fe^{3+} complex at 556 nm in the absence and presence of HPO_4^{2-}, respectively.

In order to gain an insight into the increased fluorescence intensity by 1.3-fold after addition of HPO_4^{2}, the UV-vis absorption spectra are further investigated (Fig. 5a). Upon addition of HPO_4^{2-}, the absorption peak (λ_{max}) at 450 nm gradually decreases with a hypsochromic shift to 415 nm, and a isosbestic point at 422 nm is observed, implying the formation of a new complex [N-CDs–Fe^{3+}–HPO_4^{2-}]. Meanwhile the color changes from crimson to a faint yellow. The ratiometric absorbance (A_{415}/A_{450}) presents a good linear relationship ($R^2 = 0.9982$) with the concentration of HPO_4^{2-} in a range of 0–80 μM (Fig. 5b).

The fluorescence emission spectra are further investigated under 415 nm excitation. The emission maximum (λ^{fl}_{max}) is still at 556 nm, and a very large Stokes shift of 141 nm is displayed. Moreover, the fluorescence intensity is obviously higher by 1.2-fold than that of the [N-CDs–Fe^{3+}–HPO_4^{2-}] complex under 450 nm excitation (Fig. S10a, ESI†). The recovery efficiency $[(F_0 - F)/F_0]$ presents a good linear relationship ($R^2 = 0.9991$) with the concentration of HPO_4^{2-} in the range of 0–65 μM (Fig. S10b, ESI†).

Possible interaction mechanism between the N-CDs–Fe^{3+} and HPO_4^{2-}

In addition, the FT-IR spectra are employed again for further understanding the interaction between the N-CDs–Fe^{3+} complex and HPO_4^{2} (Fig. S5b, ESI†). With the addition of Fe^{3+}, the peaks of amino groups (3388 and 1584 cm^{-1}) and carboxyl groups (3185 cm^{-1}) disappear to be replaced by a large broad peak at 3384 cm^{-1}, and a new peak of an amine salt at 2469 cm^{-1} appears,[38] suggesting that the carboxyl and amino groups all coordinate with Fe^{3+} and form the N-CDs–Fe^{3+} complex. Then addition of HPO_4^{2-} into the N-CDs–Fe^{3+} complex was continued, and the peaks of amino and carboxyl groups did not show up. The peak of an amine salt at 2469 cm^{-1} and the peak of the C–N group at 1061 cm^{-1} are enhanced, implying that a new complex of [N-CDs–Fe^{3+}–HPO_4^{2-}] is formed.

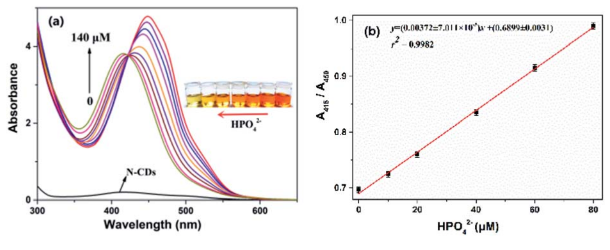

Fig. 5 (a) Absorption spectra of the N-CDs–Fe^{3+} complex in pure water with the different concentrations of HPO_4^{2-} (0–140 μM). The inset is the image of the N-CDs–Fe^{3+} complex in pure water with the increased HPO_4^{2-} from right to left under daylight. (b) Linear relationship between ratiometric absorbance (A_{415}/A_{450}) and the concentration of HPO_4^{2-}.

Moreover, the zeta potential values are also explored. The zeta potential of the N-CDs is 9.84 mV (Fig. S11a, ESI†). With the addition of Fe^{3+}, the zeta potential rises to 11.0 mV (Fig. S11b, ESI†), indicating that the contribution of the carboxyl group is larger than that of the amino group in coordination of Fe^{3+}. Then after addition of HPO_4^{2-}, the potential value reduces to 9.91 mV (Fig. S11c, ESI†), suggesting that HPO_4^{2-} is selectively bonded to the N-CDs–Fe^{3+} complex and further involved in the complicated structure of [N-CDs–Fe^{3+}–HPO_4^{2-}].

Effect of pH on the N-CDs

The influence of pH on the N-CDs is investigated in the biologically relevant pH range (HEPES, 25 mM, 5.0–9.0). As shown in Fig. S12,† the fluorescence intensity obviously increases with the increase of the pH value from 5.0 to 8.5, and then the growth tends to slow from 8.5 to 9.0, suggesting that the N-CDs could be applied well in the physiological environment at pH 7.0–7.5. Herein, the increased fluorescence intensity can be attributed to the donor-excited photoinduced electron transfer (d-PET) process. In this process, the N-CDs serve as electron donors, and the functional groups on the surface of the N-CDs, such as the amino group and carboxyl group, are electron acceptors. In an acidic solution, the nitrogen atom of the amino group is protonated (NH^+), and the LUMO energy of this acceptor becomes lower than that of the excited N-CDs, leading to a d-PET quenching process.[39,40] However, the carboxyl group is deprotonated and forms COO^- in an alkaline solution, which elevates the LUMO level by enhancing the electron density of the carboxyl group and hampers the d-PET process, resulting in a high quantum yield of the N-CDs.[41]

Selectivity of the N-CDs

The interactions between the as-fabricated N-CDs and different metal ions are also evaluated, including K^+, Na^+, Mg^{2+}, Zn^{2+}, Ca^{2+}, Ba^{2+}, Cd^{2+}, Cu^{2+}, Sr^{2+}, Pb^{2+}, Hg^{2+}, Co^{2+}, Mn^{2+}, Fe^{2+}, Al^{3+}, Cr^{3+} and Fe^{3+}, and the fluorescence properties are measured under 450 nm excitation (Fig. 6). Among these cations, only Fe^{3+} exhibits almost complete fluorescence quenching towards the N-CDs. While Cd^{2+}, Al^{3+} and Cr^{3+} have a slight quenching effect, the other cations have an ignorable quenching effect on the fluorescence intensity of the N-CDs. These results demonstrate that the as-prepared N-CDs have high sensitivity and selectivity towards Fe^{3+} over other metal ions. Similarly, only HPO_4^{2-} can further form the complex of the [N-CDs–Fe^{3+}–HPO_4^{2-}] and results in the fluorescence recovery, whereas other anions, such as Cl^- and HCO_3^- that exist in living systems, have no effect on the fluorescence enhancement.

Stability of the N-CDs

The photostability of the N-CDs is assessed by the measurement of fluorescence intensity at 556 nm under continuous exposure of ultraviolet light for 120 min. The result shows that no remarkable change is observed under the 420 nm excitation in pure water, indicating that the N-CDs have high photostability against photobleaching (Fig. S13, ESI†). Furthermore, the effects of different ionic strengths (0.0–2.0 M KCl) on the N-CDs (0.04 mg mL^{-1}) are also investigated, and there are no obvious changes in the fluorescence intensities and peak characteristics of the N-CDs (Fig. S14, ESI†), suggesting that the N-CDs have huge potential for further application in the biomedical field.

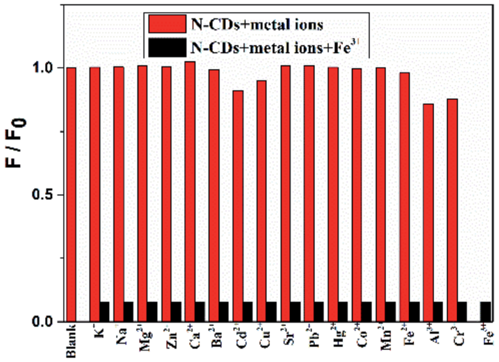

Fig. 6 Relative fluorescence intensity of the N-CDs (0.04 mg mL^{-1}) in the presence of 140 μM Fe^{3+}, and 500 μM of K^+, Na^+, Mg^{2+}, Zn^{2+}, Ca^{2+}, Ba^{2+}, Cd^{2+}, Cu^{2+}, Sr^{2+}, Pb^{2+}, Hg^{2+}, Co^{2+}, Mn^{2+}, Fe^{2+}, Al^{3+} and Cr^{3+} in an aqueous solution (pH 7.0), where F_0 and F are the fluorescence intensities of the N-CDs in the absence and the presence of various metal ions, respectively. The excitation wavelength is 450 nm.

Cellular imaging

In order to investigate the response abilities of the N-CDs to Fe^{3+} and HPO_4^{2-} in living cells, HEp-2 cells are employed and the cell cytotoxicity of the N-CDs to HEp-2 cells is assessed by MTT assay at concentrations from 0 to 1.0 mg mL^{-1} for 24 h. The result shows that the survival rate of HEp-2 cells is more than 90% even at the maximum concentration of 1.0 mg mL^{-1} (Fig. S15, ESI†), demonstrating that the N-CDs have no obvious cytotoxicity to the cells below 1.0 mg mL^{-1}, and the N-CDs could be used as a promising candidate for Fe^{3+} and HPO_4^{2-} *in vivo* detection.

Subsequently, HEp-2 cells are cultured with the N-CDs (0.5 mg mL^{-1}) for 1 h at 37 °C. After this the cells are washed with HEPES buffer solution three times and imaged with excitation at 458 nm and emissions at 500–580 nm. Then some of them are used as the control group, and the others are incubated with 140 μM of Fe^{3+} solution for 2 h. As shown in Fig. 7, the HEp-2 cells incubated with the N-CDs emit bright yellow fluorescence. However, the yellow fluorescence is extremely quenched when Fe^{3+} is introduced into the N-CD pretreated cells. After this 140 μM of HPO_4^{2-} is added into the above cells for another hour; an obvious fluorescence recovery is observed with a sensitive "on–off–on" fluorescence response. The mean fluorescence intensities are calculated using ImageJ software (Fig. 7j) and are consistent with the performance of the N-CDs in pure water. These results confirm that the as-fabricated N-CDs can be used as a nanosensor for visual monitoring of intracellular Fe^{3+} and HPO_4^{2-}, implying that the N-CDs have large potential for application as a diagnostic reagent.

Since there is little information about carbon dots that could detect Fe^{3+} and HPO_4^{2-} in the meantime, a comparison has

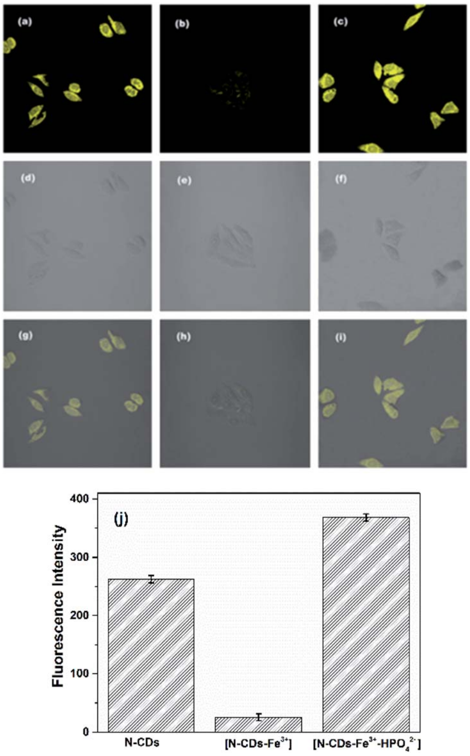

Fig. 7 Confocal fluorescence images of HEp-2 cells. (a) Incubation with 0.50 mg mL^{-1} of the N-CDs. (b) Followed by incubation with 140 μM of Fe^{3+} solution. (c) Further subsequent incubation with 140 μM of HPO_4^{2-} solution. (d–f) Bright-field images. (g–i) Merged images. (j) Mean fluorescence intensities of HEp-2 cells under different incubation conditions (data are presented as mean ± SD with replicates (n = 3)).

been made among reported carbon dots for Fe^{3+} sensing. As shown in Table S1,† the as-fabricated N-CDs show not only the maximum absorption peak (λ_{max}) at 450 nm but also a Stokes shift up to 106 nm with a very low detection limit and higher fluorescence quantum yield. As for the detection of HPO_4^{2-}, reported organic dyes for HPO_4^{2-} or $H_2PO_4^{-}$ sensing have to be employed due to few data based on carbon dots for monitoring of HPO_4^{2-}. As Table S2† shows, most of these organic dyes show UV light excitation or their Stokes shifts are very small. Even if some of them have a large Stokes shift with the excitation of visible light (ref. S33†), their extremely poor solubility in water seriously limits their application in living systems. Moreover, all of these organic dyes suffer from photobleaching and poor water solubility. In comparison with these organic dyes, the as-synthesized N-CDs exhibit not only good water solubility, biocompatibility and high photostability but also a large Stokes shift up to 106 nm with a lower detection limit of 0.80 μM for HPO_4^{2-}, implying their great potential for diverse application in the biomedical field.

Conclusions

A nanosensor based on N-doped CDs has been developed by a one-pot hydrothermal method. The average size of the N-CDs is 3.32 nm with a good crystalline structure. The N-CDs exhibit excellent water dispersibility, good biocompatibility and anti-photobleaching properties. Moreover, the N-CDs possess a large Stokes shift of 106 nm under 450 nm excitation with the fluorescence quantum yield (φ) 20%. Upon addition of Fe^{3+}, distinct fluorescence quenching is observed with an obvious color change from light yellow to crimson under daylight by the naked eye; a good linear range is presented in a range of 0–65 μM with a detection limit of 0.85 μM for Fe^{3+}. However, the quenched fluorescence could be rapidly recovered by the addition of HPO_4^{2-} which can be attributed to formation of the complex [N-CDs–Fe^{3+}–HPO_4^{2-}]. A good linear range is exhibited in the range of 0–60 μM with a detection limit of 0.80 μM for HPO_4^{2-}. Furthermore, the confocal images show that the as-prepared N-CDs could be used as a nanosensor for monitoring of intracellular Fe^{3+} and HPO_4^{2-}, demonstrating that the N-CDs have diverse potential application in the biomedical and biological fields.

Conflicts of interest

There are no conflicts to declare.

Acknowledgements

This work was financially supported by National Science Fund for Distinguished Young Scholars (21804098), Shanxi Province Science Foundation for Youths (201901D211422) and Shanxi "1331 project" Collaborative Innovation Center.

Notes and references

1 R. S. Eisenstein, *Annu. Rev. Nutr.*, 2000, **20**, 627–662.
2 R. Meneghini, *Free Radical Biol. Med.*, 1997, **23**, 783–792.
3 E. D. Weinberg, *J. Pharm. Pharmacol.*, 2006, **58**, 575–584.
4 T. A. Rouault, *Nat. Chem. Biol.*, 2006, **2**, 406–414.
5 G. Cairo and A. Pietrangelo, *Biochem. J.*, 2000, **352**, 241–250.
6 J. Kaplan, D. M. Ward and I. D. Domenico, *Int. J. Hematol.*, 2011, **93**, 14–20.
7 S. V. Torti and F. M. Torti, *Nat. Rev. Cancer*, 2013, **13**, 342–355.
8 E. L. Que, D. W. Domaille and C. J. Chang, *Chem. Rev.*, 2008, **108**, 1517–1549.
9 M. Zheng, H. Tan, Z. Xie, L. Zhang, X. Jing and Z. Sun, *ACS Appl. Mater. Interfaces*, 2013, **5**, 1078–1083.
10 A. S. Dornelles, V. A. Garcia, M. N. M. de Lima, G. Vedana, L. A. Alcalde, M. R. Bogo and N. Schröder, *Neurochem. Res.*, 2010, **35**, 564–571.
11 M. Wenzel, J. R. Hiscock and P. A. Gale, *Chem. Soc. Rev.*, 2012, **41**, 480–520.
12 S. K. Kim and J. L. Sessler, *Chem. Soc. Rev.*, 2010, **39**, 3784–3809.
13 S. Khoshniat, A. Bourgine, M. Julien, P. Weiss, J. Guicheux and L. Beck, *Cell. Mol. Life Sci.*, 2011, **68**, 205–218.
14 H. D. Kay and B. L. Guyatt, *Nature*, 1933, **131**, 468–469.
15 L. Håglin, M. Domellöf, L. Bäckman and L. Forsgren, *Clin. Nutr. ESPEN*, 2020, **37**, 93–99.

16 T. A. Couttas, N. Kain, B. Daniels, X. Y. Lim, C. Shepherd, J. Kril, R. Pickford, H. Li, B. Garner and A. S. Don, *Acta Neuropathol. Commun.*, 2014, **2**, 9.

17 J. Shangguan, D. He, X. He, K. Wang, F. Xu, J. Liu, J. Tang, X. Yang and J. Huang, *Anal. Chem.*, 2016, **88**, 7837–7843.

18 C. Yu, X. Li, F. Zeng, F. Zheng and S. Wu, *Chem. Commun.*, 2013, **49**, 403–405.

19 X. Yang, F. Cui, R. Ren, J. Sun, J. Ji, F. Pi, Y. Zhang and X. Sun, *ACS Omega*, 2019, **4**, 12575–12583.

20 J. Shen, S. Shang, X. Chen, D. Wang and Y. Cai, *Mater. Sci. Eng., C*, 2017, **76**, 856–864.

21 P. Lv, Y. Yao, H. Zhou, J. Zhang, Z. Pang, K. Ao, Y. Cai and Q. Wei, *Nanotechnology*, 2017, **28**, 165502.

22 S. A. Hill, D. Benito-Alifonso, S. A. Davis, D. J. Morgan, M. Berry and M. C. Galan, *Sci. Rep.*, 2018, **8**, 12234.

23 C. Sun, Y. Zhang, P. Wang, Y. Yang, Y. Wang, J. Xu, Y. Wang and W. W. Yu, *Nanoscale Res. Lett.*, 2016, **11**, 110.

24 H. Qi, M. Teng, M. Liu, S. Liu, J. Li, H. Yu, C. Teng, Z. Huang, H. Liu, Q. Shao, A. Umar, T. Ding, Q. Gao and Z. Guo, *J. Colloid Interface Sci.*, 2019, **539**, 332–341.

25 M. Zheng and Z. Xie, *Mater. Today Chem.*, 2019, **13**, 121–127.

26 M. Zulfajri, G. Gedda, C. J. Chang, Y. P. Chang and G. G. Huang, *ACS Omega*, 2019, **4**, 15382–15392.

27 S. K. Kailasa, S. Ha, S. H. Baek, L. M. T. Phan, S. Kim, K. Kwak and T. J. Park, *Mater. Sci. Eng., C*, 2019, **98**, 834–842.

28 J. Shangguan, J. Huang, D. He, X. He, K. Wang, R. Ye, X. Yang, T. Qing and J. Tang, *Anal. Chem.*, 2017, **89**, 7477–7484.

29 G. He, M. Xu, M. Shu, X. Li, Z. Yang, L. Zhang, Y. Su, N. Hu and Y. Zhang, *Nanotechnology*, 2016, **27**, 395706.

30 C. Fan, K. Ao, P. Lv, J. Dong, D. Wang, Y. Cai, Q. Wei and Y. Xu, *Nano*, 2018, **13**, 1850097.

31 X. Lian, K. Cheng, D. Wang, W. Zhu and X. Wang, *Int. J. Food Prop.*, 2017, **20**, S3224–S3236.

32 W. Lu, X. Gong, Z. Yang, Y. Zhang, Q. Hu, S. Shuang, C. Dong and M. M. F. Choi, *RSC Adv.*, 2015, **5**, 16972–16979.

33 M. Vedamalai, A. P. Periasamy, C. W. Wang, Y. T. Tseng, C. C. Shih and H. T. Chang, *Nanoscale*, 2014, **6**, 13119–13125.

34 L. Song, Y. Cui, C. Zhang, Z. Hu and X. Liu, *RSC Adv.*, 2016, **6**, 17704–17712.

35 J. Yu, C. Liu, K. Yuan, Z. Lu, Y. Cheng, L. Li, X. Zhang, P. Jin, F. Meng and H. Liu, *Nanomaterials*, 2018, **8**, 233.

36 R. F. Kubin and A. N. Fletcher, *J. Lumin.*, 1982, **27**, 455–462.

37 V. Singh and A. K. Mishra, *Sens. Actuators, B*, 2016, **227**, 467–474.

38 B. C. Smith, Organic Nitrogen Compounds V: Amine Salts, *Spectroscopy*, 2019, **34**, 30–37.

39 B. Turfan and E. U. Akkaya, *Org. Lett.*, 2002, **4**, 2857–2859.

40 Q. Liu, X. Niu, Y. Zhang, Y. Zhao, K. Xie, B. Yang, Q. He, S. Lv and L. Li, *Nanoscale*, 2020, **12**, 13010–13016.

41 T. Mineno, T. Ueno, Y. Urano, H. Kojima and T. Nagano, *Org. Lett.*, 2006, **8**, 5963–5966.